Bistatic High Resolution Imaging on a Monostatic Range

Wolfgang F. Herdeg*, B. Röde

Deutsche Forschungsanstalt für Luft - und Raumfahrt
Institut für Hochfrequenztechnik
W-8031 Oberpfaffenhofen Germany

ABSTRACT

Experiments measuring high resolution bistatic radar cross sections of complex objects usually require a much more sophisticated equipment than monostatic measurements since transmitter frequency and receiver oscillators have to be synchronized in order to establish coherency. This paper demonstrates the possibility to obtain information about the bistatic scattering behaviour of complex objec using a monostatic radar range. The method combines proper arrangements of large flat plates (microwave mirrors) with a high resolution imaging algorithm. In order to verify the proposed concept bistatic images of a rectangular wedge and a cube are shown and the influence of the polarization is investigated. A second possible mirror configuration offers the possibility to study the bistatic scattering behavior of a rectangular metal edge over a wide range of bistatic angles.

INTRODUCTION

In spite of the stealth issue and of general academic interest, to the authors'knowledge, quantitative experimental investigations of bistatic scattering mechanisms at basic geometrical discontinuities by high resolution microwave imaging are rare in open literature. The few experiments known to the authors were carried through on bistatic range: Mensa and Heidbreber (Mensa, 1982) employed a monochromatic radar; they varied the bistatic angle and used Kell's monostatic/bistatic equivalence theorem (Kell, 1965) in order to yield a sufficient bandwidth for the range resolution. Blanchard and Dolaty (Blanchard, 1988) exploited the conventional frequency diversity imaging technique (Farhat, 1984), for the bistatic configuration.
None of the aforementioned work investigated quantitatively the bistatic scattering mechanisms leading to distinct scattering centers in the resulting high resolution microwave images.
This paper introduces a method which allows to measure bistatic scattering phenomena, on a monostatic outdoor range. The method employs proper arrangements of large flat metal reflector plates combined with high resolution imaging (Herdeg, 1990; Herdeg, 1991).
In order to verify the proposed concepts the bistatic scattering from a rectangular edge and a metal cube is analyzed taking into account the polarization state of the transmitting and receiving antenna. A further example demonstrates a method which permits very large bistatic angles to be accessible without any loss of resolution in the image, a fact which seems to contradict the monstatic/bistatic equivalence theorem mentioned above.

1. EXPERIMENTAL SETUP

The outdoor range comprised a monostatic coherent radar capable of handling horizontally and vertically polarized pulses at any frequency in the interval from 8 to 18 GHz, a turntable about 100 m away from the radar (far field conditions for the objects used in these experiments!), screening fences between radar and turntable in order to suppress ground reflections, a 2.5 m high conical styrofoam column placed on the turntable to support the target, and a large metal reflector plate built in lightweight construction. This microwave mirror was either mounted on the styrofoam column close to the target such that both target and reflector rotated around a common axis, or the mirror was held at a fixed position while the target was rotating in front of it on the turntable. These two configurations yield different informations about the bistatic scattering phenomena involved.

* Now with Goetze AG, D-5093 Burscheid

2. METHOD OF IMAGE GENERATION

Amplitude, $S(f, \Theta)$, and phase, $\Phi(f, \Theta)$, of the backscattered signal were measured as a function of frequency, f, and aspect angle, Θ, in frequency increments of 100 MHz, and in angular increments of 0.4°, respectively.
The microwave reflectivity distribution R(x, y) of the object in the plane (x, y) was thene generated according to (Herman, 1979)

$$R(x, y) = \frac{8}{C^2} \int_{\Theta_0 - \Delta\Theta/2}^{\Theta_0 + \Delta\Theta/2} d\Theta \int_{f_0 - \Delta f/2}^{f_0 + \Delta f/2} f S(f, \Theta) \; e^{-i\Phi(f,\Theta)} \; e^{i\frac{4\pi f}{C}(x\cos\Theta + \gamma\sin\Theta)} \; df \qquad (1)$$

Here, c is the velocity of light, and Θ_0 and f_0 are center angle and center frequency, respectively, of the processing intervals of widths $\Delta\Theta$ and Δf. (x, y) are the pixel coordinates in the image plane (see Fig. 4). The (relative) phase Φ is determined by the additional path lenght of the wave between (x, y) and the radar, in respect to the path of reference.

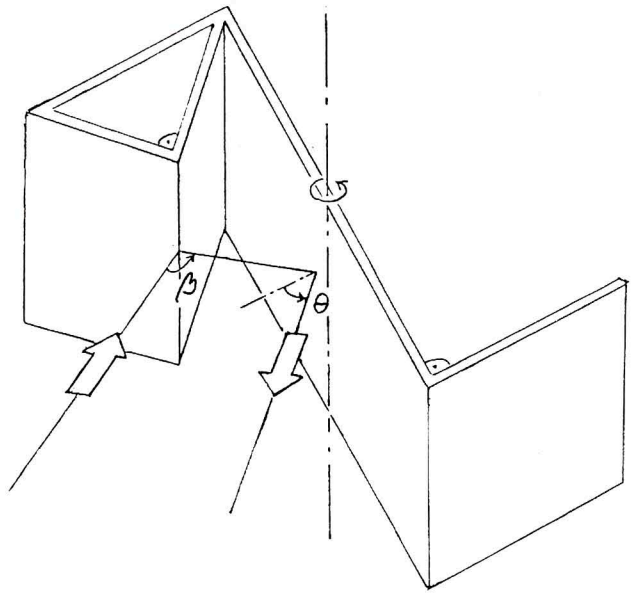

Fig. 1 - Target for the measurement of a rectangular edge in front of a corotating mirror.

3. RESULTS

Two possible arrangements of the microwave mirror were investigated. The first configuration uses a flat metal which rotates together with the target on a common platform, the axis of rotation being aligned perpendicular to the line of sight. In the experiments the scattering behavior of a rectangular metal edege being parallel to the rotational axis was studied. Combination of target (here the edge) and reflector resulted in a scattering object which is shown in Fig. 1. The dimensions of the reflector plate were 60 cm in length and 30 cm in height.
An Image of this object yields information about the bistatic scattering behaviour of the edge according to the following scattering mechanism: the wave coming from the radar is scattered at the edge into all possible directions in the plane perpendicular to the rotational axis. One of these directions enables a reflection of the edge-scattered wave at the reflector plate back to the monostatic radar. This wave path is indicated in Fig. 1. The additional path, s, the wave has to travel compared with monostatic scattering from the edge can be determined by a simple relation:

$$s = 2r\cos\Theta \qquad (2)$$

where r means the shortest distance between edge and reflector surface, $\Theta = 0^0$ denotes normal incidence onto the mirror. Because of this additional path the scattering center corresponding to this bistatic scattering mechanism shows up at the object-fixed coordinates $(x_e + r, \gamma_e)$ when (x_e, γ_e) are the coordinates of the edge. The bistatic angle belonging to the described wave path amounts to

$$\beta = 180^0 - 2\Theta \; .$$

Therefore, processing different aspect angle intervals $\Delta\Theta$ yields information about the scattering behaviour of the edge at various bistatic angles.
In order to verify these ideas, high resolution images of the object in Fig. 1 were generated from measurements for either horizontal or vertical polarization of both transmit and receive antennas (HH or VV) as shown in Fig. 2 for a process angle of 30^0 ($10^0 < \Theta < 40^0$), and a frequency interval from 8 to 14 GHz as contour plots with subsequent contour lines differing by 3 dB. The bistatic scattering center is indicated by an arrow. By shifting the center angle Θ_0 in steps of 5° with $\Delta\Theta = 30^0$ fixed, the influence of the bistatic angle on the scattering behavior of the edge can be evaluated.
The results shown in Fig. 3 are obtained by using the Huynen parameters Huynen, 1970)

$$\Upsilon = arctan\sqrt{|R_{HH}/R_{VV}|} \; , \; \nu = -\frac{1}{4} arg\,(R_{HH}/R_{VV}) \qquad (3)$$

where R_{HH} and R_{VV} are the copolar reflectivity function values taken at the location of the scattering center. The experimental values are compared with simulations based on the Uniform Geometrical Theory of Diffraction (Pathak, 1974).

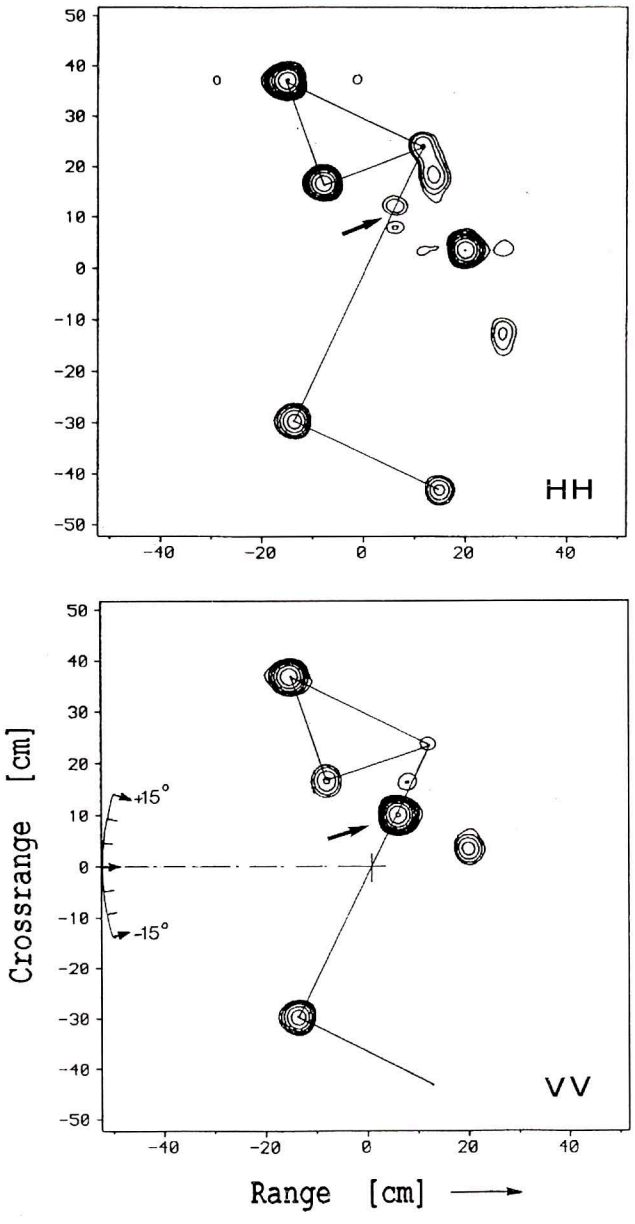

Fig. 2 - Microwave images of the target shown in Fig. 1 for HH (upper part) and VV (lower part). Neighboring contour lines differ by 3 dB.
$10^0 < \Theta < 40^0$, $8 < f < 14$ *GHz. The directions of the illuminating wave are as indicated at the lower left.*

An interesting phenomenon occurs for polarization combination HH. Though scattering is due to an isolated edge the corresponding scattering center shows splitting. It can be demonstrated that this is due to a change of sign of the corresponding edge scattering coefficient which is also responsible for the minimum of Υ in Fig. 3.
The other possible arrangement of the microwave mirror yields images which are equivalent to a conventional bistatic configuration. Since the reflector is fixed at a certain position while the target is rotating in front of it,

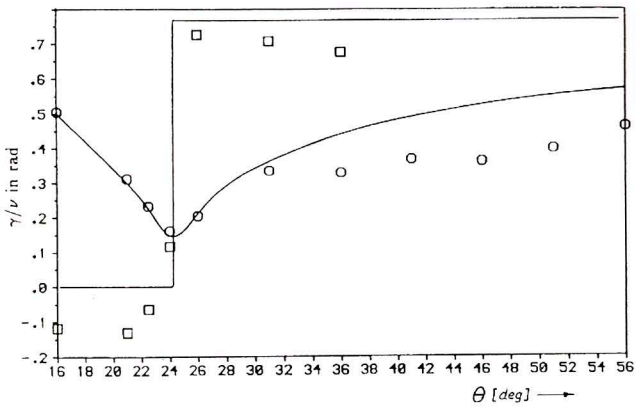

Fig. 3 - Υ and ν as function of the aspect angle. O: experimental values of Υ, []: experimental values of ν, solid lines: simulation results.

one single bistatic angle is selected. The bistatic scattering mechanism is similar to the corotating reflector configuration. For $\Theta = 0^0$ the x-axis of the object-fixed coordinate system is defined to have the direction of the bisector of the bistatic angle.
Then for bistatic scattering as indicated in Fig. 4, the extra pathlenght in respect to the monostatic signal is:

$$s = 2\,(r \sin(\beta/2) + (x_0 \cos\Theta + y_0 \sin\Theta)\cos(\beta/2))\ . \quad (4)$$

The same result without the constant term $r \sin(\beta/2)$ would be obtained for a conventional bistatic range. Since the constant term can be included in the reference path complete correspondence exists. Nevertheless high resolution imaging has to be employed since the monostatic scattering contribution (together with several further interactions with the reflector) interferes with the bistatic contribution of interest.

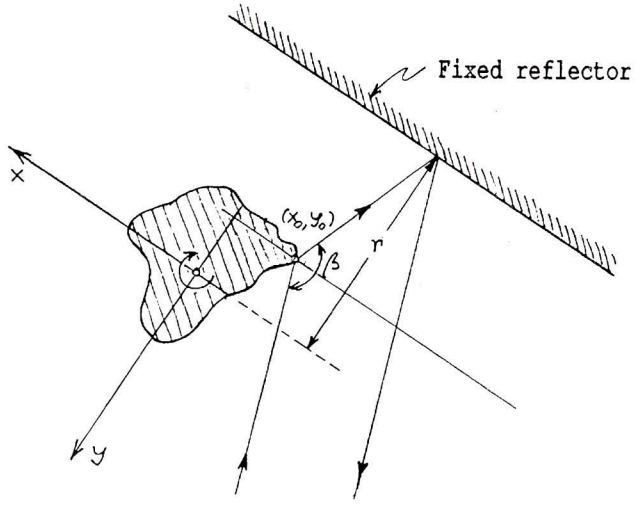

Fig. 4 - Measurement geometry for the fixed plate arrangement.

An example of this imaging geometry is given in Fig. 5. Shown is the microwave image of a cube of sidelenght 30 cm for polarization combination HH and VV at a bistatic angle of 81°. An aspect angle interval of $\Delta\,\Theta = 30^0$ and a frequency interval from 12 to 18 GHz was used to process the image.

The contour of the cube has been indicated. The extended scattering center in the image is due to a further interaction process of the wave with the fixed reflector plate. There are only two edges lie in the shadow region of the cube. It is also interesting to note that the dimension of the cube is reduced by a factor cos 40.5° according to the reduced resolution in a conventional bistatic imaging configuration. Fig. 6 shows an image with two diffraction sources, one of these is observed under a very high bistatic angle.

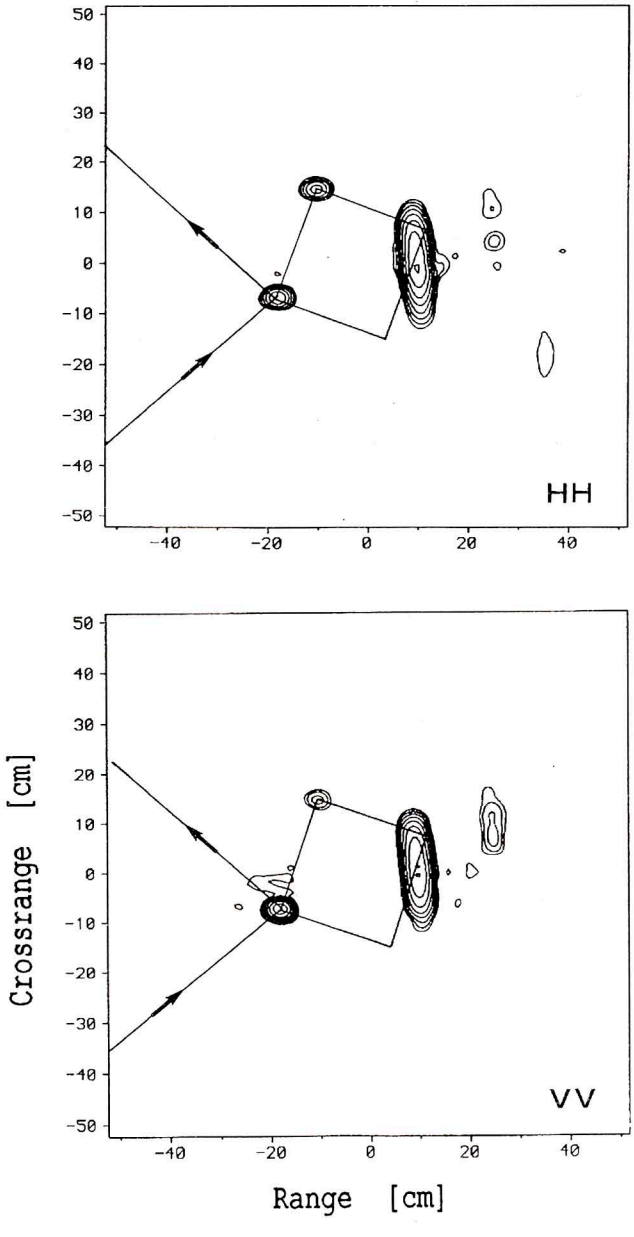

Fig. 5 - Microwave images of a cube of sidelength 30 cm. Bistatic angle: 81°, 5° < Θ < 35°, 12 < *f* < 18 *HHz for HH (upper part) and VV (lower part). Neighboring contour lines differ by 3 dB. The big intensity blob on the right side of the cube comes from a more complicated ray path of the bistatic specular reflection of the illuminated cube face (triple reflection).*

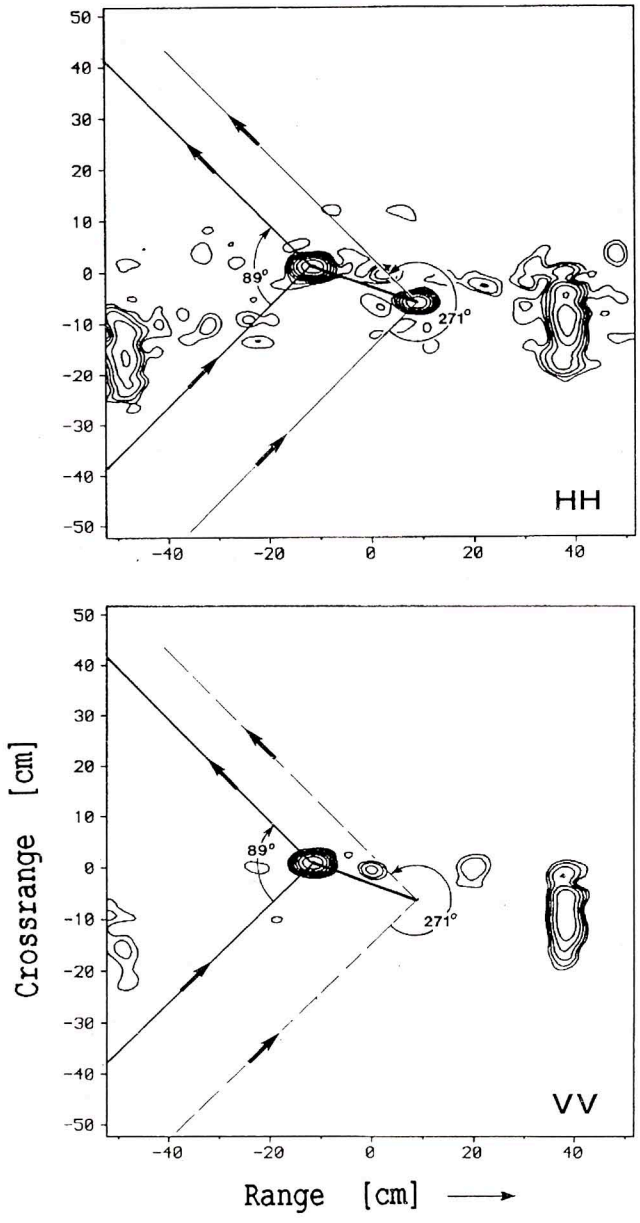

Fig. 6 - Bistatic microwave image of a rectangular plate, thickness: 0.8 cm. Interval of aspect angle: 95° < Θ < 125°. *Frequency range:* 13 *GHz* < *f* < 18 *GHz.*

CONCLUSION

It has been demonstrated that it is possible to obtain information about the bistatic scattering behaviour of individual scattering sources on a complex object by combining a monostatic radar range with properly arranged reflector plates and using a high resolution imaging algorithm.

Two different measurement configurations have been analysed. The corotating mirror has the advantage that the resolution of the image is indipendent of the actual bistatic angle. Moreover by rotating the target together with the mirror, a large range of bistatic measurement geometry. There are however also disadvantages. If a large object is to be investigated it may be difficult to handle the large mirror. For small bistatic angles the reflector plate has to be very large, too, in order to obtain a reflection point.

REFERENCES

Blanchard A.J., and Dolaty M., 1988, Bistatic frequency diverse imaging of complex scattering targets. In: Proceedings of IGARSS'88 Symposium, Edinburgh, Scotland, 13-16 Sept. 1988, 311.

Farhat N.H., Werner C.L., and Chu T.H., 1984, Prospects of three-dimensional projective and tomographic imaging radar networks. Radio Science, 19, 1347.

Herdeg W.F., and Wendel H., 1990, Bistatic high resolution imaging on monostatic range. Electron. Lett., 26, 1476.

Herdeg W.F., and Wendel H., 1991, Bistatic scattering on a monostatic radar range. ETT, 2, 459.

Herman G.T., 1979, Image Reconstruction from Projections (New York: Springer).

Huynen J.R., 1970, Phenomenological Theory of Radar Targets, Ph.D. dissertation, Technical Univ., Delft, The Netherlands.

Kell R.E., 1965, On the derivation of bistatic RCS from monostatic measurements. Proc. IEEE, 53, 983.

Mensa D., and Heidbreder G., 1982, Bistatic synthetic aperture radar imaging of rotating objects. IEEE Trans. AES, 18, 423.

Pathakm P.M., and Kouyoumjiana, R.G., 1974, A uniform geometrical theory of diffraction for an edge in a perfectly conducting surface. Proc. IEEE, 62, 1448.